MOLECULAR CLUSTER MAGNETS

JEFFREY R. LONG

Department of Chemistry, University of California, Berkeley, CA 94720, USA
E-mail: jlong@cchem.berkeley.edu

Molecular clusters with a high spin ground state and a large negative axial zero-field splitting possess an intrinsic energy barrier for spin reversal that results in slow relaxation of the magnetization. The characteristics of $[Mn_{12}O_{12}(MeCO_2)_{16}(H_2O)_4]$—the first example of such a single-molecule magnet—leading up to this behavior are described in detail. Other clusters known to exhibit an analogous behavior are enumerated, consisting primarily of oxo-bridged species containing Mn^{III}, Fe^{III}, Ni^{II}, V^{III}, or Co^{II} centers as a source of anisotropy. The progress to date in controlling the structures and magnetic properties of transition metal-cyanide clusters as a means of synthesizing new single-molecule magnets with higher spin-reversal barriers is summarized. In addition, the phenomenon of quantum tunneling of the magnetization, which has been unambiguously demonstrated with molecules of this type, is explained. Finally, potential applications involving high-density information storage, quantum computing, and magnetic refrigeration are briefly discussed.

1 Introduction

Over the course of the past decade, a rapidly increasing number of molecular clusters have been shown to exhibit magnetic bistability. These species, dubbed single-molecule magnets, possess a combination of high spin S and axial anisotropy D in the ground state that leads to an energy barrier U for reversing the direction of their magnetization. The ensuing slow magnetic relaxation observed at low temperatures is in many ways analogous to the behavior of a superparamagnetic nanoparticle below its blocking temperature [1].

With 2-30 transition metal centers and diameters in the 0.5-2 nm regime, established single-molecule magnets reside at the smaller end of the spectrum of nanostructured materials. As molecular compounds, they can generally be isolated in pure form and crystallized, permitting the precise determination of atomic structure via X-ray crystallography. Hence, with essentially no size dispersion, these species exhibit well-defined and remarkably reproducible physical properties. This, along with the massively parallel production scheme associated with solution-based molecular assembly reactions, provides impetus for the current optimism surrounding the development of spin-based molecular electronic devices. Other applications envisioned for such molecular magnets include high-density information storage, quantum computing, and magnetic refrigeration. Moreover, these clusters are positioned at the frontier between molecular and bulk magnetism, allowing study of new physical phenomena such as quantum tunneling of the magnetization.

Herein, the state of the nascent field of molecular cluster magnets is

In *Chemistry of Nanostructured Materials*; Yang, P., Ed.; World Scientific Publishing: Hong Kong, 2003.

summarized, with an eye toward elucidating new and existing challenges. In view of the considerable effort devoted to this area of research of late, surprisingly few review articles on the subject are presently available [2-5].

2 A Mn_{12} Cluster Magnet

In 1980, Lis reported the synthesis and structure of $[Mn_{12}O_{12}(MeCO_2)_{16}(H_2O)_4]\cdot 2MeCO_2H\cdot 4H_2O$, a compound containing an unprecedented dodecanuclear cluster with the disc-shaped geometry depicted in Figure 1 [6]. Its structure features a central $Mn^{IV}{}_4O_4$ cubane unit surrounded by a ring of eight Mn^{III} centers connected through bridging oxo ligands. Bridging acetate and terminal water ligands passivate the surface, such that each Mn center possesses an approximate octahedral coordination environment. Variable temperature magnetic susceptibility data were also reported by Lis, along with the prescient observation that "such a complicated dodecameric unit should have interesting magnetic properties".

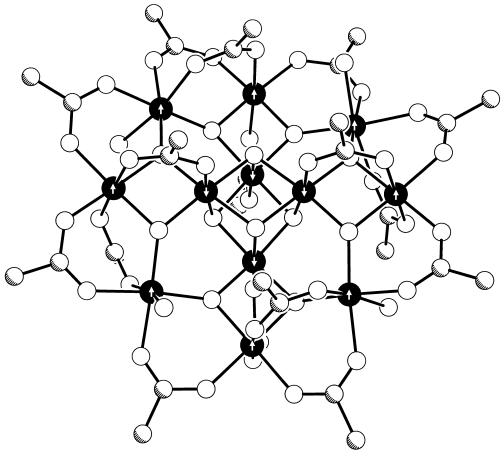

Figure 1. Structure of the disc-shaped cluster $[Mn_{12}O_{12}(MeCO_2)_{16}(H_2O)_4]$ [6]. Black, shaded, and white spheres represent Mn, C, and O atoms, respectively; H atoms are omitted for clarity. White arrows indicate relative orientations of local spins in the ground state; note that the four central Mn^{IV} centers have a lower spin ($S = {}^3/_2$) than the eight outer Mn^{III} centers ($S = 2$).

More than a decade later, magnetization data for this compound collected at high magnetic field strengths and low temperatures were interpreted as indicating an $S = 10$ ground state with significant axial anisotropy [7,8]. Coordinated by weak-field oxo donor ligands, the Mn^{IV} and Mn^{III} centers possess the electron configurations $t_{2g}{}^3e_g{}^0$ and $t_{2g}{}^3e_g{}^1$, imparting local spins of $S = {}^3/_2$ and $S = 2$, respectively. The total spin of the ground state can then be understood as arising from a situation in which

the spins of the four central Mn^{IV} centers are all aligned antiparallel to the spins of the eight outer Mn^{III} centers, to give $S = |(4 \times {}^{3}/_{2}) + (8 \times -2)| = 10$ (see Figure 1). Reduced magnetization curves for the compound were found to deviate significantly from a simple Brillouin function, suggesting that the $S = 10$ ground state is subject to a substantial zero-field splitting. Indeed, fits to the magnetization data indicate an axial zero-field splitting parameter with a magnitude of $|D| = 0.5$ cm^{-1}. High-field, high-frequency EPR spectra are consistent with this value, and further indicate the sign of D to be negative.

The negative axial zero-field splitting removes the degeneracy in the M_S levels of the ground state, placing the higher magnitude levels lower in energy, as depicted in Figure 2. Together with the selection rule of $\Delta M_S = \pm 1$ for allowed transitions, this results in an energy barrier U separating the two lowest energy levels of $M_S = +10$ and $M_S = -10$. In general, for an integral spin state, the energy barrier will be $U = S^2|D|$, while for a half-integral spin state it will be $U = (S^2 - {}^{1}/_{4})|D|$. Thus, for the $S = 10$ ground state of the Mn_{12} cluster, we have a spin-reversal energy barrier of $U = S^2|D| = 10^2|-0.5$ cm$^{-1}| = 50$ cm^{-1}. Note that a positive D value would result in the $M_S = 0$ level being lowest in energy, such that there is no energy cost for losing direction of the spin (i.e., in going, for example, from to $M_S = +10$ to $M_S = 0$).

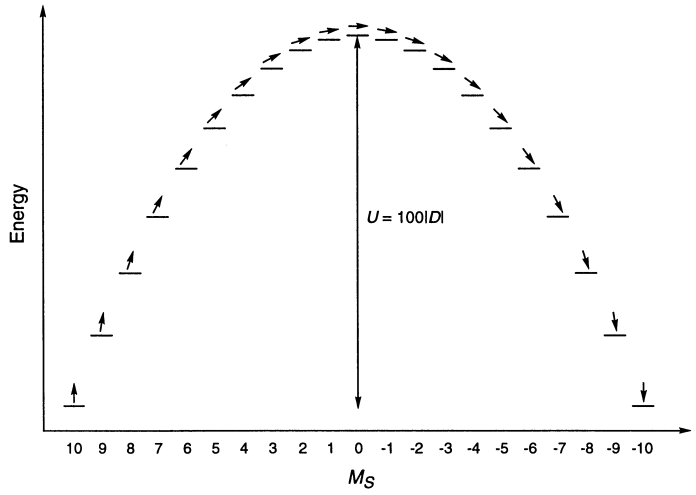

Figure 2. Energy level diagram for an $S = 10$ ground state with a negative axial zero-field splitting, D, in the absence of an applied magnetic field. Arrows represent the relative orientation of the spin with respect to the easy axis of the molecule. As indicated, the spin reversal barrier is given by $U = S^2|D| = 100|D|$. For $[Mn_{12}O_{12}(MeCO_2)_{16}(H_2O)_4]$, $D = -0.5$ cm^{-1}, resulting in a barrier of $U = 50$ cm^{-1}.

As a consequence of the energy barrier U intrinsic to its ground state, the magnetization of the Mn_{12} cluster can be pinned along one direction, and then relaxes only slowly at very low temperatures. This effect is readily probed through

AC magnetic susceptibility measurements, which provide a direct means of gauging the relaxation rate. Here, the susceptibility of a sample is measured using a weak magnetic field (usually of ca. 1 G) that switches direction at a fixed frequency. As the switching frequency increases and starts to approach the relaxation rate for the magnetization within the molecules, the measured susceptibility—referred to as the in-phase or real component of the AC susceptibility and symbolized as χ'—begins to diminish. Accordingly, the portion of the susceptibility that cannot keep up with the switching field—referred to as the out-of-phase or imaginary component of the AC susceptibility and symbolized as χ''—increases. If just a single relaxation process is operational, then a plot of χ'' versus temperature will display a peak with a maximum at the temperature where the switching of the magnetic field matches the relaxation rate, $1/\tau$, for the magnetization of the molecules. Furthermore, since $1/\tau$ increases with temperature, this peak should shift to higher temperature when the switching frequency is increased. As shown in Figure 3, such behavior has indeed been observed for $[Mn_{12}O_{12}(MeCO_2)_{16}(H_2O)_4]\cdot 2MeCO_2H\cdot 4H_2O$ [8]. More precisely, the relaxation time for the magnetization in a single-molecule magnet can be expected to follow an Arrhenius relationship:

$$\tau = \tau_0 e^{(U_{eff}/k_B T)} \qquad (1)$$

where the preexponential term τ_0 can be thought of as the relaxation attempt frequency. Thus, a plot of $\ln\tau$ versus $1/T$ should be linear, with the slope and intercept permitting evaluation of U_{eff} and τ_0. Analysis of data for the $[Mn_{12}O_{12}(MeCO_2)_{16}(H_2O)_4]$ cluster in this manner gave $U_{eff} = 42$ cm^{-1} and $\tau_0 = 2.1 \times 10^{-7}$ s [9]. Note that, as is generally the case, the effective energy barrier U_{eff} obtained is slightly lower than the intrinsic spin reversal barrier U calculated from S

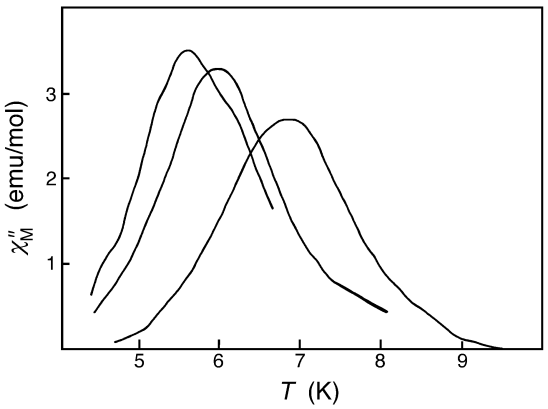

Figure 3. Schematic representation of the out-of-phase component of the molar AC magnetic susceptibility observed for a polycrystalline sample of $[Mn_{12}O_{12}(MeCO_2)_{16}(H_2O)_4]\cdot 2MeCO_2H\cdot 4H_2O$ in zero applied DC field (adapted from reference 8). From left to right, peaks correspond to data collected in an AC field oscillating at a frequency of 55, 100, and 500 Hz, respectively.

and *D*, owing to the effects of quantum tunneling of the magnetization (see Section 5). Importantly, AC susceptibility measurements performed on the analogous $[Mn_{12}O_{12}(EtCO_2)_{16}(H_2O)_4]$ cluster dissolved in polystyrene reveal the same behavior, indicating that the slow magnetic relaxation is indeed associated with individual clusters and is not a bulk phenomenon [10].

The slow relaxation of the magnetization in a single-molecule magnet also leads to magnetic hysteresis. Figure 4 depicts a hysteresis loop collected for a sample of $[Mn_{12}O_{12}(MeCO_2)_{16}(H_2O)_4]\cdot 2MeCO_2H\cdot 4H_2O$ at 2.1 K [11]. This hysteresis has a substantially different origin from that in an ordered ferromagnet. Here, rather than inducing domain wall motion, increasing the applied magnetic field shifts the relative energies of the M_S levels (see Figure 2), decreasing the thermal activation barrier for reversing spin direction and thereby accelerating the relaxation process. As a consequence, the coercivity of the sample changes dramatically with temperature. For example, at 2.6 K, the hysteresis loop shown in Figure 4 narrows to one having a coercive field of less than 0.5 T [11]. As explained below in Section 5, the unusual steps apparent in the hysteresis curve are due to quantum tunneling of the magnetization.

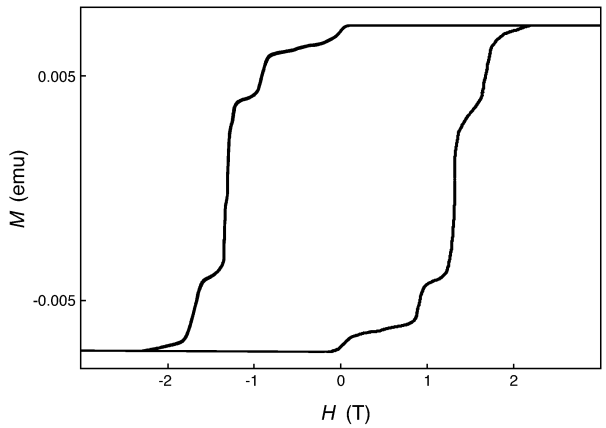

Figure 4. Schematic representation of a magnetic hysteresis loop observed for a single crystal of $[Mn_{12}O_{12}(MeCO_2)_{16}(H_2O)_4]\cdot 2MeCO_2H\cdot 4H_2O$ at 2.1 K (adapted from reference 11).

The presence of an energy barrier for reversing spin orientation suggests the possibility of storing a bit of information as the direction of the spin in an individual molecule (in addition to the other applications discussed in Section 6). With $U_{eff} \approx 40$ cm^{-1}, the Mn_{12} cluster exhibits a magnetization relaxation half-life of more than 2 months at 2 K; however, above 4 K this half-life is dramatically reduced and magnetic hysteresis is no longer observed [9]. Thus, in order for these molecules to be capable of storing information at more practical temperatures there

is a clear need for clusters possessing a larger spin reversal barrier U. To meet this challenge, one would like to identify or synthesize molecules bearing ground states with exceptionally high spin S and a large negative axial anisotropy D.

3 Other Oxo-Bridged Cluster Magnets

Since the discovery of the remarkable magnetic properties of the Mn_{12} cluster, much effort has been devoted to searching for other examples of molecules exhibiting such behavior. The fruits of that effort are enumerated in Table 1 [7-9,12-40], with the clusters arranged in order of decreasing U_{eff}. In most cases, U_{eff} was established using AC susceptibility measurements, while S and D were determined by fitting magnetization data and high-field EPR spectra [41], respectively. A variety of other physical techniques can also be of utility in probing the magnetic anisotropy of these systems, including high-field torque magnetometry and the use of micro-SQUID arrays [42,43].

Table 1. Examples of Single-Molecule Magnets.

	S	D (cm^{-1})	U_{eff} (cm^{-1})	ref
$[Mn_{12}O_{12}(CH_2BrCO_2)_{16}(H_2O)_4]$	10		56[a]	12
$[Mn_{12}O_{12}(CHCl_2CO_2)_8(Bu^tCH_2CO_2)_8(H_2O)_4]$	10	-0.45	50	13
$[Mn_{12}O_{12}(CHCl_2CO_2)_8(EtCO_2)_8(H_2O)_4]$	10	-0.42	49	13
$[Mn_{12}O_{12}(MeCHCHCO_2)_{16}(H_2O)_4]$	10	-0.44	45	14
$[Mn_{12}O_{12}(p\text{-}PhC_6H_4CO_2)_{16}(H_2O)_4]$	10	-0.44	45	14
$[Mn_{12}O_{12}(p\text{-}MeC_6H_4CO_2)_{16}(H_2O)_4]$[b]	10		44	15
$[Mn_{12}O_{12}(MeCO_2)_{16}(H_2O)_4]$	10	-0.5	42	7-9
$[Mn_{12}O_{12}(MeCO_2)_8(Ph_2PO_2)_8(H_2O)_4]$	10	-0.41	42	16
$[Mn_{12}O_{12}(PhCO_2)_{16}(H_2O)_4]^{1-}$	$^{19}/_2$	-0.44	40	17
$[Mn_{30}O_{24}(OH)_8(Bu^tCH_2CO_2)_{32}(H_2O)_2(MeNO_2)_4]$	7	-0.79	39[c]	18
$[Mn_{12}O_{12}(CHCl_2CO_2)_{16}(H_2O)_4]^{2-}$	10	-0.27	27[c]	19
$[Mn_{12}O_{12}(p\text{-}MeC_6H_4CO_2)_{16}(H_2O)_4]$[d]	10		26	15
$[Mn_{12}O_8Cl_4(PhCO_2)_8(hmp)_6]$[e]	7	-0.6	21	20
$[Mn_9O_7(MeCO_2)_{11}(thme)(py)_3(H_2O)_2]$[f]	$^{17}/_2$	-0.29	19	21
$[Fe_8O_2(OH)_{12}(tacn)_6]^{8+}$[g]	10	-0.19	15	22
$[V_4O_2(EtCO_2)_7(bpy)_2]^{1+}$[h]	3	-1.5	14[c]	23
$[Mn_4(MeCO_2)_2(pdmH)_6]^{2+}$[i]	8	-0.24	12	24
$[Mn_4O_3(p\text{-}MeC_6H_4CO_2)_4(dbm)_3]$[j]	$^{9}/_2$	-0.62	12[c]	25
$[Mn_4(hmp)_6Br_2(H_2O)_2]^{2+}$[e]	9	-0.35	11	26
$[(Me_3tacn)_6MnMo_6(CN)_{18}]^{2+}$[k]	$^{13}/_2$	-0.33	10	27
$[Fe_{19}O_6(OH)_{14}(metheidi)_{10}(H_2O)_{12}]^{1+}$[l]	$^{33}/_2$	-0.035	9.5[c]	28
$[Mn_4O_2(MeO)_3(PhCO_2)_2L_2(MeOH)]^{2+}$[m]	$^{7}/_2$	-0.77	9.2[c]	29

$[Mn_4O_3Br(MeCO_2)_3(dbm)_3]^j$	$^9/_2$	-0.50	8.3	30
$[Mn_4O_3Cl(MeCO_2)_3(dbm)_3]^j$	$^9/_2$	-0.53	8.2	31
$[Ni_{12}(chp)_{12}(MeCO_2)_{12}(H_2O)_6(THF)_6]^n$	12	-0.047	7	32
$[Mn_{10}O_4(biphen)_4Br_{12}]^{4-\,o}$	12	-0.037	4.9	33
$[(tetren)_6Ni_6Cr(CN)_6]^{9+\,p}$	$^{15}/_2$		4.2	34
$[Fe_{10}Na_2O_6(OH)_4(PhCO_2)_{10}(chp)_6(H_2O)_2$-$(MeCO_2)_2]^n$	11		3.7	35
$[Ni_4(MeO)_4(sal)_4(MeOH)_4]^q$	4		3.7	36
$[Mn_9(O_2CEt)_{12}(pdm)_2(pdmH)_2(C_{14}H_{16}N_2O_4)_2]^i$	$^{11}/_2$	-0.11	3.1	37
$[Ni_{21}(OH)_{10}(cit)_{12}(H_2O)_{10}]^{16-\,r}$	3		2.9	38
$[Fe_4(MeO)_6(dpm)_6]^s$	5	-0.2	2.4	39
$[Fe_2F_9]^{3-}$	5	-0.15	1.5	40

[a]This sample also displays a second relaxation process with U_{eff} = 23 cm^{-1}. [b]Crystallized with three water solvate molecules. [c]Estimated value (U), based upon S and D; typically, the measured value (U_{eff}) is somewhat lower, owing to quantum tunneling of the magnetization. [d]Crystallized with one *p*-$MeC_6H_4CO_2H$ solvate molecule. [e]hmpH = 2-hydroxymethylpyridine. [f]thmeH$_3$ = 1,1,1-tris(hydroxymethyl)ethane. [g]tacn = 1,4,7-triazacyclononane. [h]bpy = 2,2′-bipyridine. [i]pdmH$_2$ = pyridine-2,6-dimethanol. [j]dbmH = dibenzoylmethane. [k]Me$_3$tacn = *N*,*N*′,*N*″-trimethyl-1,4,7-triazacyclononane. [l]metheidiH$_3$ = *N*-(1-hydroxynethylethyl)iminodiacetic acid. [m]L = 1,2-bis(2,2′-bipyridine-6-yl)ethane. [n]biphen = 2,2′-biphenoxide. [o]chp = 6-chloro-2-pyridonate. [p]tetren = tetraethylenepentamine. [q]salH = salicylaldehyde. [r]cit^{4-} = citrate. [s]dpmH = dipivaloylmethane.

A quick inspection of Table 1 reveals that by far the majority (30 out of 33) of the known single-molecule magnets are clusters in which the metal centers are bridged by oxygen donor atoms. Of these, most are manganese-containing species, with only a few clusters featuring iron or nickel and just one containing vanadium. Ground state spins range from $S = 3$ to $S = {}^{33}/_2$, while the D values measured vary between -0.037 and -1.5 cm^{-1}. Significantly, the highest values of U_{eff} are still held by $[Mn_{12}O_{12}(RCO_2)_{16}(H_2O)_4]$ clusters with an S = 10 ground state and the core structure depicted in Figure 1.

The all-important magnetic anisotropy of these clusters stems from anisotropy in the electronic structure of the individual metal centers, which in turn arises from spin-orbit coupling. Metal ions with orbital angular momentum and a strong tendency to undergo a Jahn-Teller distortion are particularly suitable for generating a large overall D value. For example, the manganese-oxo clusters listed in Table 1 all contain octahedral Mn^{III} centers with a $t_{2g}{}^3e_g{}^1$ electron configuration. In the $[Mn_{12}O_{12}(MeCO_2)_{16}(H_2O)_4]$ cluster (see Figure 1) the Mn^{III} centers all display a distorted coordination environment consisting of a tetragonal elongation, which occurs roughly perpendicular to the disc of the molecule and coincident with its easy axis. Indeed, variants of the Mn_{12} cluster structure in which some of the tetragonal elongation axes are not so aligned show significantly reduced spin-reversal energy barriers [15,16]. The anisotropy in other metal-oxo single-molecule magnets results from pseudooctahedral V^{III} ($t_{2g}{}^2e_g{}^0$), Fe^{III} ($t_{2g}{}^3e_g{}^2$), or Ni^{II} ($t_{2g}{}^6e_g{}^2$) centers. Very recently, $[Co_4(hmp)_4(MeOH)_4Cl_4]$ (hmpH = hydroxymethylpyridine), an S = 6

ground-state cluster containing pseudooctahedral Co^{II} ($t_{2g}^5 e_g^2$) centers, was reported to behave as a single-molecule magnet with an exceptionally large overall anisotropy estimated at $D = -3$ cm^{-1} [44]. It is worth noting that metal centers such as V^{III} and Co^{II}, which typically display an individual anisotropy where D is positive, can in fact give rise to clusters with a negative overall D value [23,44]. In fact, systems involving these two metal ions in particular would seem to hold considerable promise for the development of new single-molecule magnets with high spin-reversal barriers. Unfortunately, not much is yet understood about how to control or predict the overall magnetic anisotropy of a cluster, even knowing the nature of the anisotropy associated with its constituent metal centers [45].

The molecules listed in Table 1 represent only a rather low percentage of the metal-oxo clusters that have been prepared and investigated for their magnetic properties. It is not sufficient for a cluster simply to have a large number of interacting paramagnetic metal centers, since very frequently these will conspire to produce a ground state of low or zero net spin. For the most part, the clusters are synthesized in one-step self-assembly reactions, from which it is usually impossible to predict the structure of the product *a priori*. The difficulty lies in the enormous structural variability encountered in metal-oxo cluster systems, which, while fascinating from many perspectives, waylays most attempts at developing rational approaches to their synthesis. For a given cluster product considerable variation is possible in the nuclearity, the M-O-M angles (90-180°), and the coordination number of the bridging oxygen atoms (2-6). Moreover, the pairwise magnetic exchange interactions within a cluster are highly sensitive to geometry, making it all but impossible to predict the magnetic properties of a complex metal-oxo cluster. Thus, the discovery of new metal-oxo single-molecule magnets remains very much a serendipitous process.

4 Cyano-Bridged Clusters

As an alternative system where some control over structures and magnetic properties can be anticipated, a number of researchers have turned to metal-cyanide clusters. In a bridging coordination mode, cyanide binds only two metal centers and exhibits a distinct preference for a linear geometry. Thus, assembly reactions can be set up with the expectation that the product will feature linear M'-CN-M moieties. Moreover, given this bridging arrangement, it is possible to predict the nature of the magnetic exchange interactions between M' and M (see Figure 5) [46,47]. Assuming an octahedral coordination geometry for both metal centers, unpaired electrons in orbitals of compatible symmetry ($t_{2g} + t_{2g}$ or $e_g + e_g$) will couple antiferromagnetically, while those in orthogonal orbitals ($t_{2g} + e_g$) will couple ferromagnetically. The antiferromagnetic interaction is typically stronger than the ferromagnetic interaction, and will dominate the superexchange in a competitive

situation. Furthermore, the strength of the exchange interaction depends critically upon the degree of overlap between the metal- and cyanide-based orbitals, and, consequently, is high when the radially-extended *d* orbitals of low-valent early transition metals are involved.

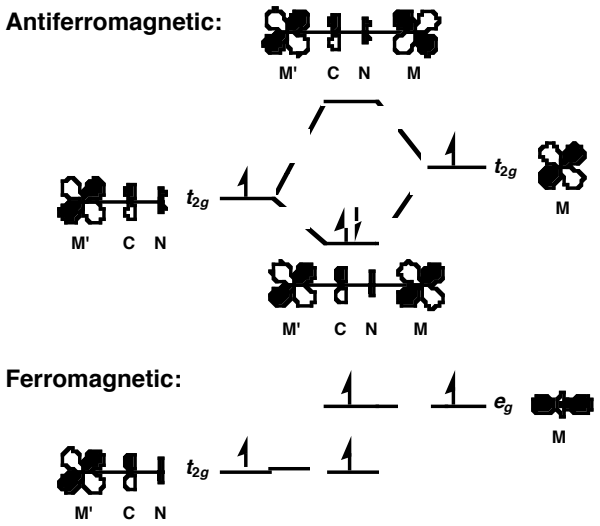

Figure 5. Orbital interactions across a bridging cyanide ligand giving rise to magnetic superexchange. Upper: Unpaired electrons in symmetry compatible t_{2g} orbitals interact through cyanide π^* orbitals, resulting in antiferromagnetic coupling (via the Pauli exclusion principle). In actuality, this is a bit of an oversimplification, as electronic structure calculations indicate that the π orbitals of cyanide are responsible to nearly the same extent [47]. Lower: Unpaired electrons from incompatible metal-based orbitals leak over into orthogonal cyanide-based orbitals, resulting in ferromagnetic coupling (via Hund's rules).

Much of the confidence in being able to control the structures and magnetic properties of metal-cyanide clusters is predicated by extensive investigations into magnetic Prussian blue type solids [46-54]. These compounds have proven to exhibit highly adjustable magnetic behavior, and are generally synthesized via aqueous assembly reactions of the following type.

$$x[M(H_2O)_6]^{y+} + y[M'(CN)_6]^{x-} \rightarrow M_x[M'(CN)_6]_y \cdot zH_2O \qquad (2)$$

The resulting structures are based on an extended cubic lattice of alternating M and M' centers connected through linear cyanide bridges. Two different metal sites are present in the framework, one in which the metal, M', is coordinated by the carbon end of cyanide and experiences a strong ligand field, and another in which the metal, M, is coordinated by the nitrogen end of cyanide and experiences a weak ligand field. Recognition of how the aforementioned factors influence magnetic superexchange

through cyanide has enabled chemists to produce solids of this type with bulk magnetic ordering temperatures as high as 376 K [54].

A simple strategy for synthesizing molecular metal-cyanide clusters parallels that employed in reaction 2, but utilizes blocking ligands to hinder formation of an extended solid. The level of structural control possible is illustrated with the assembly of clusters consisting of just one of the fundamental cubic cage units comprising the Prussian blue structure type. Here, a tridentate ligand such as 1,4,7-triazacyclononane (tacn) is employed to block three *fac* sites in the octahedral coordination sphere of each precursor complex.

$$4[(tacn)M(H_2O)_3]^{x+} + 4[(tacn)M'(CN)_3]^{y-} \rightarrow [(tacn)_8M_4M'_4(CN)_{12}]^{4(x-y)+} \quad (3)$$

As in the reaction 2, the nitrogen end of the cyanide ligand displaces water to form linear M'-CN-M linkages. Now, however, the tacn ligands, which are not so readily displaced owing to the chelate effect, prevent growth of an extended Prussian blue framework, and direct formation of a discrete molecular cube. Successful implementation of this strategy has been demonstrated with the reaction between $[(tacn)Co(H_2O)_3]^{3+}$ and $[(tacn)Co(CN)_3]$ in boiling aqueous solution to form the cubic $[(tacn)_8Co_8(CN)_{12}]^{12+}$ cluster depicted in Figure 6 [55,56]. Analogous clusters capped by cyclopentadienyl, a mixture of cyclopentadienyl and carbonyl, or a mixture of 1,3,5-triaminocyclohexane and water ligands have also been reported [57-59].

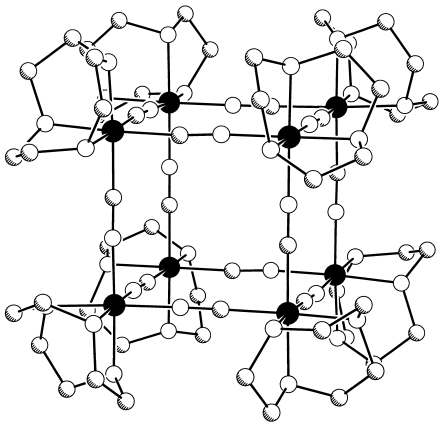

Figure 6. Structure of the cubic cluster $[(tacn)_8Co_8(CN)_{12}]^{12+}$, as crystallized in $[(tacn)_8Co_8(CN)_{12}]$-$(C_7H_7SO_3)\cdot 24H_2O$ [56]. Black, shaded, and white spheres represent Co, C, and N atoms, respectively; H atoms are omitted for clarity.

In distinct contrast to the situation with metal-oxo clusters, once a new metal-cyanide cluster has been discovered, one can be reasonably confident that it will be

possible to substitute other transition metal ions having similar geometric proclivities into the structure. This provides a potent means for attempting to manipulate the strength of the magnetic exchange coupling, the overall spin of the ground state, and even the magnetic anisotropy within a cluster. The maximum spin ground state attainable for a cubic $M_4M'_4(CN)_{12}$ cluster, however, is $S = 10$, corresponding, for example, to the case where ferromagnetic coupling is expected to arise between $M = Ni^{II}$ ($t_{2g}^6 e_g^2$) and $M' = Cr^{III}$ ($t_{2g}^3 e_g^0$). Note that this is the same as the spin in the original Mn_{12} single-molecule magnet.

To produce the exceptionally large spin states ultimately sought in single-molecule magnets, it is necessary to develop methods for constructing higher nuclearity clusters in which an even greater number of metal centers are magnetically coupled. One simple idea for accomplishing this is to carry out assembly reactions with a blocking ligand on only one of the components in reaction 3. Accordingly, the following reaction performed in boiling aqueous solution was found to yield a fourteen-metal cluster (Me_3tacn = *N*,*N'*,*N"*-trimethyl-1,4,7-triazacyclononane) [56].

$$8[(Me_3tacn)Cr(CN)_3] + 6[Ni(H_2O)_6]^{2+} \rightarrow [(Me_3tacn)_8Cr_8Ni_6(CN)_{24}]^{12+} \quad (4)$$

As depicted in Figure 7, the product exhibits a core structure consisting of a cube of eight Cr^{III} centers connected through cyanide bridges to six Ni^{II} centers positioned just above the faces of the cube. Note, however, that the carbon ends of the cyanide ligands are now bound to Ni^{II}, whereas they were initially bound to Cr^{III} in the reactants. Apparently, in the course of heating the reaction, sufficient thermal energy

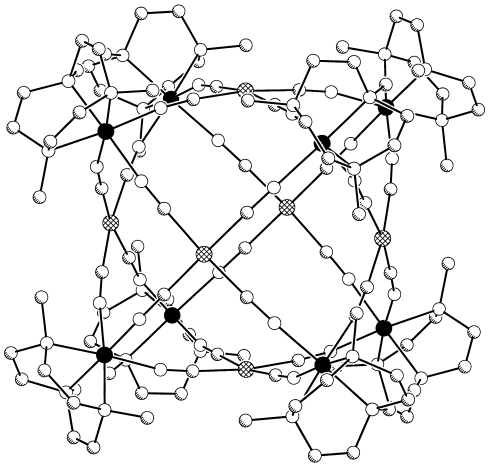

Figure 7. Structure of the face-centered cubic cluster $[(Me_3tacn)_8Cr_8Ni_6(CN)_{24}]^{12+}$, as crystallized in $[(Me_3tacn)_8Cr_8Ni_6(CN)_{24}](NO_3)\cdot 54H_2O$ [56]. Black, crosshatched, shaded, and white spheres represent Cr, Ni, C, and N atoms, respectively; H atoms are omitted for clarity.

is available to induce isomerization of the cyanide ligand to give the thermodynamically-preferred Ni^{II}-CN-Cr^{III} orientation. Unfortunately, this has the added effect of driving the Ni^{II} centers toward a square planar coordination geometry with a low-spin diamagnetic electron configuration, thereby destroying any exchange coupling with the surrounding Cr^{III} centers. The isomerization of cyanide can be forestalled, however, by carrying out reaction 4 at -40 °C in methanol, resulting in a metastable cluster of nominal formula $[(Me_3tacn)_8(H_2O)_x(MeOH)_yNi_6Cr_8(CN)_{24}]^{12+}$. Magnetic susceptibility and magnetization data collected for samples containing this cluster are consistent with the expected ferromagnetic coupling between Cr^{III} and high-spin Ni^{II}, giving rise to an $S = 18$ ground state.

Similar approaches have led to numerous other molecular metal-cyanide clusters [52,60]. The highest nuclearity geometries yet uncovered occur in the tetracapped edge-bridged cubic $[(Me_3tacn)_{12}Cr_{12}Ni_{12}(CN)_{48}]^{12+}$ and double face-centered cubic $[(Me_3tacn)_{14}Cr_{14}Ni_{13}(CN)_{48}]^{20+}$ clusters recently reported [61]. Although these both contain diamagnetic Ni^{II} centers as a consequence of isomerization of the cyanide ligands, isolation of the high-spin form of the latter species would presumably result in a cluster with an $S = 34$ ground state. While a spin state of this magnitude has not yet been realized, many other high-spin metal-cyanide clusters have now been characterized. Table 2 presents these in order of decreasing S. Topping the list are body-centered, face-capped cubic clusters produced through reactions between Mn^{2+} ions and $[M(CN)_8]^{3-}$ (M = Mo, W) complexes in methanol or ethanol. Magnetic susceptibility and magnetization data for $[(EtOH)_{24}Mn_9W_6(CN)_{48}]$ clearly indicate antiferromagnetic coupling between the Mn^{II} and W^{V} centers to give an $S = {}^{39}/_{2}$ ground state [63]. Surprisingly, the analogous $[(MeOH)_{24}Mn_9Mo_6(CN)_{48}]$ cluster instead appears to exhibit ferromagnetic coupling and an $S = {}^{51}/_{2}$ ground state, although there may still be some question as to whether desolvation has complicated the measurements [62]. Regardless, these are the highest spin ground states yet observed for a molecular cluster, surpassing the previous record of $S = {}^{33}/_{2}$ held by $[Fe_{19}O_6(OH)_{14}(heidi)_{10}(H_2O)_{12}]^{1+}$ (heidiH$_3$ = $N(CH_2COOH)_2(CH_2CH_2OH)$) [81].

In most cases, Table 2 also lists the coupling constant J characterizing the exchange interactions through cyanide within the clusters. Here, an exchange Hamiltonian of the pairwise form $\hat{H} = -2J\hat{S}_1 \cdot \hat{S}_2$ has been employed. Occasionally, researchers will use an alternative convention where the exchange Hamiltonian is instead of the form $\hat{H} = -J\hat{S}_1 \cdot \hat{S}_2$, making it extremely important to cite which convention has been adopted for the sake comparing J values. Note that with either form, a negative J value indicates antiferromagnetic coupling, while a positive J value indicates ferromagnetic coupling. These magnetic coupling constants are normally obtained by fitting the temperature dependence of the measured magnetic susceptibility using a model exchange Hamiltonian that incorporates all of the pairwise exchange parameters for the pertinent cluster geometry. With metal-cyanide clusters, it is usually sufficient to include only the exchange between metal centers

Table 2. Examples of High-Spin Metal-Cyanide Clusters.

	S	J (cm^{-1})[a]	ref
$[(MeOH)_{24}Mn^{II}_{9}Mo^{V}_{6}(CN)_{48}]$	$^{51}/_{2}$	+	62
$[(EtOH)_{24}Mn^{II}_{9}W^{V}_{6}(CN)_{48}]$	$^{39}/_{2}$	-	63
$[(Me_3tacn)_8(H_2O)_x(MeOH)_yNi^{II}_{6}Cr^{III}_{8}(CN)_{24}]^{12+}$ [b]	18	+	56
$[(TrispicMeen)_6Mn^{II}_{6}Cr^{III}(CN)_6]^{9+}$ [c]	$^{27}/_{2}$	-4.0	64
$[(dmptacn)_6Mn^{II}_{6}Cr^{III}(CN)_6]^{9+}$ [d]	$^{27}/_{2}$	-5	65
$[(MeOH)_{24}Ni^{II}_{9}M^{V}_{6}(CN)_{48}]$ (M = Mo, W)	12	ca. +16	66
$[(IM2\text{-}py)_6Ni^{II}_{3}Cr^{III}_{2}(CN)_{12}]$[e]	9	+5	67
$[(tetren)_6Ni^{II}_{6}Cr^{III}(CN)_6]^{9+}$ [f]	$^{15}/_{2}$	+8.4	68
$[(IM2\text{-}py)_6Ni^{II}_{3}Fe^{III}_{2}(CN)_{12}]$[e]	7	+3.4	69
$[(Me_3tacn)_6Mn^{II}Cr^{III}_{6}(CN)_{18}]^{2+}$ [b]	$^{13}/_{2}$	-3.1	70
$[(Me_3tacn)_6Mn^{II}Mo^{III}_{6}(CN)_{18}]^{2+}$ [b]	$^{13}/_{2}$	-6.7	27
$[(bpy)_6(H_2O)_2Mn^{II}_{3}W^{V}_{2}(CN)_{16}]$[g]	$^{13}/_{2}$	-6.0	71
$[(HIM2\text{-}py)_6Ni^{II}_{3}Cr^{III}_{2}(CN)_{12}]$[e]	6	+6.8[e]	72
$[(tach)_4(H_2O)_{12}Ni^{II}_{4}Fe^{III}_{4}(CN)_{12}]^{8+}$ [h]	6	+6.1	59
$[(Me_3tacn)_2(cyclam)_3(H_2O)_2Ni^{II}_{3}Mo^{III}_{2}(CN)_6]^{6+}$ [bi]	6	+8.5, +4.0	73
$[(5\text{-}Brsalen)_2Mn^{III}_{2}Fe^{III}(CN)_6]^{1-}$ [j]	$^{9}/_{2}$	+2.3	74
$[(Tp)_3(H_2O)_3Fe^{III}_{4}(CN)_9]$[k]	4	+	75
$[(Me_3tacn)_2(cyclam)Ni^{II}Cr^{III}_{2}(CN)_6]^{2+}$ [bi]	4	+10.9	56
$[(bpm)_6Ni^{II}_{3}Fe^{III}_{2}(CN)_{12}]$[l]	4	+5.3, -1.7	76
$[(bpy)_6Ni^{II}_{3}Fe^{III}_{2}(CN)_{12}]$[g]	4	+3.9	77
$[(Me_3tacn)_2(cyclam)Ni^{II}Mo^{III}_{2}(CN)_6]^{2+}$ [bi]	4	+17.6	73
$[(H_2L)_2Ni^{II}_{2}Fe^{III}_{3}(CN)_{18}]^{1-}$ [m]	$^{7}/_{2}$	+2.1	78
$[(tach)(H_2O)_{15}Ni^{II}_{3}Fe^{III}(CN)_3]^{6+}$ [h]	$^{7}/_{2}$	+0.8	59
$[(dmbpy)_4(IM2\text{-}py)_2Cu^{II}_{2}Fe^{III}_{2}(CN)_4]^{6+}$ [n]	3	+4.9	79
$[(edma)_3Cu^{II}_{3}Cr^{III}(CN)_6]$[o]	3	+9.2	80

[a]For clusters where it has not been explicitly determined, only the sign of J is given. [b]Me_3tacn = *N*,*N*′,*N*″-trimethyl-1,4,7-triazacyclononane. [c]TrispicMeen = *N*,*N*′,*N*″-(tris(2-pyridylmethyl)-*N*′-methylethan)1,2-diamine. [d]dmptacn = 1,4-bis(2-methylpyridyl)-1,4,7-triazacyclononane. [e]IM2-py = 2-(2-pyridyl)-4,4,5,5-tetramethyl-4,5-dihydro-1*H*-imidazolyl-1-oxy. [f]tetren = tetraethylenepentamine. [g]bpy = 2,2'-bipyridine. [h]tach = 1,3,5-triaminocyclohexane. [i]cyclam = 1,4,8,11-tetraazacyclotetradecane. [j]5-Brsalen = *N*,*N*′-ethylenebis(5-bromosalicylideneiminato) dianion. [k]Tp = hydrotris(1-pyrazolyl)borate. [l]bpm = bis(1-pyazolyl)methane. [m]L = 3,10-bis(2-aminoethyl)-1,3,6,8,10,12-hexaazacyclotetradecane. [n]dmbpy = 4,4'-dimethyl-2,2'-bipyridine. [o]edma = ethylenediaminemonoacetate.

directly connected to each other through a cyanide bridge. For the clusters in Table 2, measured J values range in magnitude from 0.8 to 17.6 cm^{-1}. Overall, the coupling tends to be a bit weaker than observed for oxo-bridged clusters. Given an appropriate choice of metal ions, however, the coupling through a cyanide bridge can be much stronger, and the highest J value yet observed is -113 cm^{-1}, occurring in the dinuclear molybdenum(III) complex $[Mo_2(CN)_{11}]^{5-}$ [82].

Ultimately, the strength of the magnetic exchange coupling is quite important if single-molecule magnets are to be produced that retain their unusual properties at higher temperatures. This is because J dictates how high excited spin states are above the ground state, and if these are close in energy then the spin reversal barrier may be compromised by their thermal population. Thus, identification of a linear bridging ligand that could be utilized in place of cyanide and deliver stronger magnetic exchange coupling would be of considerable value. A little-explored means of potentially achieving molecules with well-isolated, high-spin ground states involves use of electron delocalization to generate strong magnetic exchange coupling via a double-exchange mechanism [83].

Although high-spin, the clusters occupying the top six entries of Table 2 all approximate O_h symmetry. While this does not necessarily preclude development of magnetic anisotropy (since a very slight structural distortion could accompany magnetic polarization), it certainly might act against it. Indeed, none of these very high-spin molecules have been shown to exhibit single-molecule magnet behavior. Consequently, the development of strategies for synthesizing high-nuclearity metal-cyanide clusters with a more anisotropic overall geometry presents an important goal. An example of a high-spin species with a lower-symmetry geometry is the trigonal prismatic cluster $[(Me_3tacn)_6MnCr_6(CN)_{18}]^{2+}$ depicted in Figure 8 [70]. This molecule has an $S = {}^{13}/_2$ ground state, and was obtained serendipitously from a reaction between Mn^{2+} and $[(Me_3tacn)Cr(CN)_3]$ in aqueous solution. Although it displays a unique molecular axis, the cluster still does not behave as a single-molecule magnet, owing to the negligible single-ion anisotropy associated with its Mn^{II} ($t_{2g}{}^3e_g{}^2$) and Cr^{III} ($t_{2g}{}^3e_g{}^0$) centers.

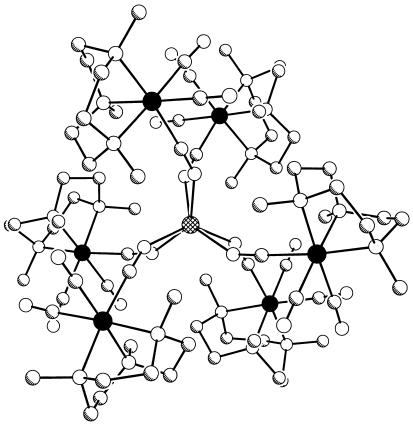

Figure 8. Structure of the trigonal prismatic cluster $[(Me_3tacn)_6MnCr_6(CN)_{18}]^{2+}$, as crystallized in $K[(Me_3tacn)_6MnCr_6(CN)_{18}](ClO_4)_3$ [70]. Black, crosshatched, shaded, and white spheres represent Mo, Mn, C, and N atoms, respectively; H atoms are omitted for clarity.

In fact, very few of the clusters listed in Table 2 contain metal ions likely to contribute to a large overall magnetic anisotropy. As stated previously, however, it is frequently possible to substitute other metal ions into a known metal-cyanide geometry, thereby potentially altering the ground state anisotropy. Accordingly, a straightforward approach to producing single-molecule magnets might be to replace the metal centers of the lower-symmetry clusters in Table 2 with ions known to deliver the anisotropy in metal-oxo single-molecule magnets, particularly Mn^{III}, V^{III}, and Co^{II}. Another idea is simply to move down the column in the periodic table and utilize second- or third-row transition metal ions. Since spin-orbit coupling is a relativistic phenomenon, this will generally enhance significantly any single-ion anisotropy. For example, while $[Cr(acac)_3]$ (acac = acetylacetonate) has an axial zero-field splitting of $|D| = 0.59$ cm^{-1} [84], $[Mo(acac)_3]$ exhibits a large negative D value of -6.3 cm^{-1} [85]. Hence, replacing the Cr^{III} centers in a cluster with Mo^{III} might be expected to impart magnetic anisotropy while preserving the spin of the ground state. As an added advantage, the strength of the magnetic exchange coupling in the cluster should also increase, owing to the more diffuse valence d orbitals of Mo^{III}. Synthesis of the octahedral complex $[(Me_3tacn)Mo(CN)_3]$ [73] enabled a demonstration of precisely these effects. Simply employing it in place of $[(Me_3tacn)Cr(CN)_3]$ in the preparation established for the trigonal prismatic cluster $[(Me_3tacn)_6MnCr_6(CN)_{18}]^{2+}$ (see Figure 8), resulted in an isostructural product containing $[(Me_3tacn)_6MnMo_6(CN)_{18}]^{2+}$ [27]. Incorporating Mo^{III}, this cluster still has a ground state of $S = {}^{13}/_2$, but with an axial zero-field splitting of $D = -0.33$ cm^{-1} and an exchange coupling constant that has increased from -3.1 cm^{-1} to -6.7 cm^{-1}. AC susceptibility measurements indeed show it to behave as a single-molecule magnet with $U_{eff} = 10$ cm^{-1}.

Ultimately, it is anticipated that similar substitutions in higher-spin metal-cyanide clusters may lead to new examples of single-molecule magnets with significantly enhanced spin-reversal energy barriers.

5 Quantum Tunneling of the Magnetization

Owing to the extremely high level of interest from physicists, a substantial body of literature already exists on quantum tunneling of the magnetization in single-molecule magnets. Rather than attempting a complete overview of the subject here, we will give only a very basic description of the phenomenon.

In 1996, two groups of researchers independently proposed an explanation for the unusual steplike features apparent in the magnetic hysteresis loops obtained from samples of $[Mn_{12}O_{12}(MeCO_2)_{16}(H_2O)_4]\cdot 2MeCO_2H\cdot 4H_2O$ [11,86,87]. Inspection of Figure 4 reveals, for example, four steps on each side of the hysteresis loop collected at 2.1 K. These steps originate from a loss of spin polarization in the

molecules due to tunneling of the magnetization through the energy barrier U rather than simple thermal activation. This tunneling only occurs with the resonant alignment of two (or more) M_S levels on the left and right sides of the energy diagram displayed in Figure 2. As shown, in zero applied magnetic field each M_S = +N level is aligned with the corresponding M_S = -N level, fulfilling the resonance condition. Indeed, the first step in the hysteresis loop shown in Figure 4 arises at H = 0. The tunneling does not necessarily transpire between the pair of levels lowest in energy, and in fact the probability of tunneling increases as one progresses upward toward M_S = 0. Thus, much of the loss of magnetization is a result of thermally-assisted tunneling between higher energy levels. As the strength of the applied magnetic field is increased, the M_S levels shift in energy, with the lower levels going up on one side and down on the other until eventually the spin reversal barrier disappears. Between these two extremes lie a number of field strengths at which a resonance occurs that again permits tunneling of the magnetization. Accordingly, the positions of the steps in the hysteresis loops can be used to map out the M_S energy levels of the ground state.

Certain differences in the rate of tunneling are observed between the various single-molecule magnets. The distinction can be particularly evident at extremely low temperatures, where the thermal energy no longer assists the tunneling process. For example, this temperature-independent regime is much more readily attained in the cluster $[Fe_8O_2(OH)_{12}(tacn)_6]^{8+}$ (which also has an S = 10 ground state) than in the Mn_{12} cluster [88]. The discrepancy has been attributed to the greater transverse component to the anisotropy of the former molecule. That is, the Fe_8 cluster shows a significantly larger value for the rhombic zero-field splitting parameter E (as well as fourth order terms), resulting in a greater degree of mixing between the $M_S = \pm N$ levels, which, in turn, facilitates tunneling [89].

6 Potential Applications

Several applications for single-molecule magnets have been envisioned.

Perhaps the most obvious of these is their potential future use as magnetic data storage media. Here, the idea is that an individual molecule would be capable of storing a single bit of binary information as the direction of its magnetization—i.e, with spin up representing, say, a 0 and spin down representing a 1. With a diameter of just 1-2 nm, this could lead to surface storage densities as high as 200,000 Gbits/in^2, approximately three orders of magnitude greater than can be achieved with current magnetic alloy film technology. Data storage density is of particular import in computer hard drives, where the distance between bits of information places constraints upon the speed and efficiency of the computer. Thus, the use of self-assembled monolayers of single-molecule magnets as a storage media could one day lead to extremely fast computer hard drives. Clearly, a significant challenge that

must be met in order for this idea to come to fruition is the development of methods for reading and writing such miniscule magnetic moments. Another challenge, and one that is more amenable to chemists, lies in the synthesis of molecules having larger spin reversal barriers U, which would then permit storage of information at more accessible temperatures. As discussed previously, this entails constructing molecules possessing a well-isolated ground state with a very high spin S and a large negative axial zero-field splitting D. In addition, since quantum tunneling of the magnetization could contribute to the loss of information, one would ideally like these molecules to exhibit no transverse anisotropy.

Recently, it has been shown theoretically that single-molecule magnets could be used as the memory components in quantum computing [90-92]. A single crystal of the molecules could potentially serve as the storage unit of a dynamic random access memory device in which fast electron spin resonance pulses are used to read and write information [90]. This application would take advantage of the quantized transitions between the numerous M_S levels in the ground state of a single-molecule magnet, but must be implemented at very low temperature (below ca. 1 K) to avoid transitions due to spin-phonon interactions. Such a device would have an estimated clock speed of 10 GHz and could store any number between 0 and 2^{2S-2} (= 2.6 × 10^5 for S = 10). Thus, to maximize the capacity of the memory, one would like to have a single-molecule magnet with as large a spin S as feasible. In addition, to ensure that resolution of the level structure within the ground state manifold is maintained, it is important for the magnitude of D also to be large.

Finally, it has been suggested that single-molecule magnets might be of utility as low-temperature refrigerants via the magnetocaloric effect [92,93]. This application would take advantage of the large entropy change that occurs upon application of a magnetic field to a sample of randomized spins. Since each cluster magnet is identical, the change occurs only over a very narrow temperature window centered at its blocking temperature (3 K for the Mn_{12} cluster). In order to extend the range of accessible refrigeration temperatures, single-molecule magnets with higher blocking temperatures (i.e., with larger spin-reversal energy barriers U) would be of value.

7 Acknowledgments

This work was funded by NSF Grant No. CHE-0072691. I thank Ms. J. J. Sokol for helpful discussions.

References

1. Gatteschi D. and Sessoli R., Assembling magnetic blocks or how long does it take to reach infinity? In *Magnetism: A Supramolecular Function*, ed. Kahn O. (Kluwer, Dordrecht, 1996) pp. 411-430.
2. Eppley H. J., Aubin S. M. J., Wemple M. W., Adams D. M., Tsai H.-L., Grillo V. A., Castro S. L., Sun Z., Folting K., Huffman J. C., Hendrickson D. N. and Christou G., Single-molecule magnets: characterization of complexes exhibiting out-of-phase ac susceptibility signals, *Mol. Cryst. Liq. Cryst.* **305** (1997) pp. 167-179.
3. Gatteschi D., Sessoli R. and Cornia A., Single-molecule magnets based on iron(III) oxo clusters, *Chem. Commun.* (2000) pp. 725-732.
4. Gatteschi D., Single molecule magnets: a new class of magnetic materials, *J. Alloys Compd.* **317-318** (2001) pp. 8-12.
5. Hendrickson D. N., Christou G., Ishimoto H., Yoo J., Brechin E. K., Yamaguchi A., Rumberger E. M., Aubin S. M. J., Sun Z. and Aromi G., Molecular nanomagnets, *Mol. Cryst. Liq. Cryst.* **376** (2002) pp. 301-313.
6. Lis T., Preparation, structure, and magnetic properties of a dodecanuclear mixed-valence manganese carboxylate, *Acta Crystallogr. B* **36** (1980) pp. 2042-2046.
7. Caneschi A., Gatteschi D., Sessoli R., Barra A. L., Brunel L. C. and Guillot M., Alternating current susceptibility, high field magnetization, and millimeter band EPR evidence for a ground $S = 10$ state in $[Mn_{12}O_{12}(CH_3COO)_{16}(H_2O)_4]\cdot 2CH_3COOH\cdot 4H_2O$, *J. Am. Chem. Soc.* **113** (1991) pp. 5873-5874.
8. Sessoli R., Tsai H.-L., Schake A. R., Wang S., Vincent J. B., Folting K., Gatteschi D., Christou G. and Hendrickson D. N., High-spin molecules: $[Mn_{12}O_{12}(CH_3COO)_{16}(H_2O)_4]$, *J. Am. Chem. Soc.* **115** (1993) pp. 1804–1816.
9. Sessoli R., Gatteschi D., Caneschi A. and Novak M. A., Magnetic bistability in a metal-ion cluster, *Nature* **365** (1993) pp. 141-143.
10. Eppley H. J., Tsai H.-L., deVries N., Folting K., Christou G. and Hendrickson D. N., High-spin molecules: unusual magnetic susceptibility relaxation effects in $[Mn_{12}O_{12}(O_2CEt)_{16}(H_2O)_3]$ ($S = 9$) and the one-electron reduction product $(PPh_4)[Mn_{12}O_{12}(O_2CEt)_{16}(H_2O)_4]$ ($S = {}^{19}/_2$), *J. Am. Chem. Soc.* **117** (1995) pp. 301-317.
11. Thomas L., Lionti F., Ballou R., Gatteschi D., Sessoli R. and Barbara B., Macroscopic quantum tunnelling of magnetization in a single crystal of nanomagnets, *Nature* **383** (1996) pp. 145-147.
12. Tsai H.-L., Chen D.-M., Yang C.-I, Jwo T.-Y., Wur C.-S., Lee G.-H. and Wang Y., A single-molecular magnet: $[Mn_{12}O_{12}(O_2CCH_2Br)_{16}(H_2O)_4]$, *Inorg. Chem. Commun.* **4** (2001) pp. 511-514.
13. Soler M., Artus P., Folting K., Huffman J. C., Hendrickson D. N. and Christou G., Single-molecule magnets: preparation and properties of mixed-

carboxylate complexes $[Mn_{12}O_{12}(O_2CR)_8(O_2CR[]_8(H_2O)_4]$, *Inorg. Chem.* **40** (2001) pp. 4902-4912.
14. Ruiz-Molina D., Gerbier P., Rumberger E., Amabilino D. B., Guzei I. A., Folting K., Huffman J. C., Rheingold A., Christou G., Veciana J. and Hendrickson D. N., Characterization of nanoscopic $[Mn_{12}O_{12}(O_2CR)_{16}(H_2O)_4]$ single-molecule magnets: physicochemical properties and LDI- and MALDI-TOF mass spectrometry, *J. Mater. Chem.* **12** (2002) pp. 1152-1161.
15. Aubin S. M. J., Sun Z., Eppley H. J., Rumberger E. M., Guzei I. A., Folting K., Gantzel P. K., Rheingold A. L., Christou G. and Hendrickson D. N., Single-molecule magnets: Jahn-Teller isomerism and the origin of two magnetization relaxation processes in Mn_{12} complexes, *Inorg. Chem.* **40** (2001) pp. 2127-2146.
16. Boskovic C., Pink M., Huffman J. C., Hendrickson D. N. and Christou G., Single-molecule magnets: ligand-induced core distortion and multiple Jahn-Teller isomerism in $[Mn_{12}O_{12}(O_2CMe)_8(O_2PPh_2)_8(H_2O)_4]$, *J. Am. Chem. Soc.* **123** (2001) pp. 9914-9915.
17. Aubin S. M. J., Sun Z., Pardi L., Krzystek J., Folting K., Brunel L.-C., Rheingold A. L., Christou G. and Hendrickson D. N., Reduced anionic Mn_{12} molecules with half-integer ground states as single-molecule magnets, *Inorg. Chem.* **38** (1999) pp. 5329-5340.
18. Soler M., Rumberger E., Folting K., Hendrickson D. N. and Christou G., Synthesis, characterization and magnetic properties of $[Mn_{30}O_{24}(OH)_8(O_2CCH_2-C(CH_3)_3)_{32}(H_2O)_2(CH_3NO_2)_4]$: the largest manganese carboxylate cluster, *Polyhedron* **20** (2001) pp. 1365-1369.
19. Soler M., Chandra S. K., Ruiz D., Davidson E. R., Hendrickson D. N. and Christou G., A third isolated oxidation state for the Mn_{12} family of single-molecule magnets, *Chem. Commun.* (2000) pp. 2417-2418.
20. Boskovic C., Brechin E. K., Streib W. E., Folting K., Bollinger J. C., Hendrickson D. N. and Christou G., Single-molecule magnets: a new family of Mn_{12} clusters of formula $[Mn_{12}O_8X_4(O_2CPh)_8L_6]$, *J. Am. Chem. Soc.* **124** (2002) pp. 3725-3736.
21. Brechin E. K., Soler M., Davidson J., Hendrickson D. N., Parsons S., Christou G., A new class of single-molecule magnet: $[Mn_9O_7(OAc)_{11}(thme)(py)_3(H_2O)_2]$ with an S = 17/2 ground state, *Chem. Commun.* (2002) pp. 2252-2253.
22. Barra A.-L., Debrunner P., Gatteschi D., Schulz C. E. and Sessoli R., Superparamagnetic-like behavior in an octanuclear iron cluster, *Europhys. Lett.* **35** (1996) pp. 133-138.
23. Castro S. L., Sun Z., Grant C. M., Bollinger J. C., Hendrickson D. N. and Christou G., Single-molecule magnets: tetranuclear vanadium(III) complexes with a butterfly structure and an S = 3 ground state, *J. Am. Chem. Soc.* **120** (1998) pp. 2365-2375.

24. Yoo J., Brechin E. K., Yamaguchi A., Makano M., Huffman J. C., Maniero A. L., Brunel L.-C., Awage K., Ishimoto H., Christou G. and Hendrickson D. N., Single-molecule magnets: a new class of tetranuclear manganese magnets, *Inorg. Chem.* **39** (2000) pp. 3615-3623.
25. Aliaga N., Folting K., Hendrickson D. N. and Christou G., Preparation and magnetic properties of low symmetry $[Mn_4O_3]$ complexes with S = 9/2, *Polyhedron* **20** (2001) pp. 1273-1277.
26. Yoo J. Y., Yamaguchi A., Nakano M., Krzystek J., Streib W. E., Brunel L.-C., Ishimoto H., Christou G. and Hendrickson D. N., Mixed-valence tetranuclear manganese single-molecule magnets, *Inorg. Chem.* **40** (2001) pp. 4604-4616.
27. Sokol J. J., Hee A. G. and Long J. R., A cyano-bridged single-molecule magnet: slow magnetic relaxation in a trigonal prismatic $MnMo_6(CN)_{18}$ cluster, *J. Am. Chem. Soc.* **124** (2002) pp. 7656–7657.
28. Goodwin J. C., Sessoli R., Gatteschi D., Wernsdorfer W., Powell A. K. and Heath S. L., Towards nanostructured arrays of single molecule magnets: new Fe oxyhydroxide clusters displaying high ground state spins and hysteresis, *J. Chem. Soc., Dalton Trans.* (2000) pp. 1835-1840.
29. Sañudo E. C., Grillo V. A., Knapp M. J., Bollinger J. C., Huffman J. C., Hendrickson D. N. and Christou G., Tetranuclear manganese complexes with dimer-of-dimer and ladder structures from the use of a bis-bipyridyl ligand, *Inorg. Chem.* **41** (2002) pp. 2441-2450.
30. Andres H., Basler R., Güdel H.-U., Aromí G., Christou G., Büttner H. and Rufflé B., Inelastic neutron scattering and magnetic susceptibilities of the single-molecule magnets $[Mn_4O_3X(OAc)_3(dbm)_3]$ (X = Br, Cl, OAc, and F): variation of the anisotropy along the series.
31. Aubin S. M. J., Dilley N. R., Pardi L., Krzystek J., Wemple M. W., Brunel L.-C., Maple M. B., Christou G. and Hendrickson D. N., Resonant magnetization tunneling in the trigonal pyramidal $Mn^{IV}Mn^{III}_3$ complex $[Mn_4O_3Cl(O_2CCH_3)_3(dbm)_3]$, *J. Am. Chem. Soc.* **120** (1998) pp. 4991-5004.
32. Cadiou C., Murrie M., Paulsen C., Villar V., Wernsdorfer W. and Winpenny R. E. P., Studies of a nickel-based single molecule magnet: resonant quantum tunelling in an S = 12 molecule, *Chem. Commun.* (2001) pp. 2666-2667.
33. Barra A. L., Caneschi A., Goldberg D. P. and Sessoli R., Slow magnetic relaxation of $[Et_3NH][Mn(CH_3CN)(H_2O)_2][Mn_{10}O_4(biphen)_4Br_{12}]$ (biphen = 2,2□-biphenoxide) at very low temperature, *J. Solid State Chem.* **145** (1999) pp. 484-487.
34. Vernier N., Bellesa G., Mallah T. and Verdaguer M., Nonlinear magnetic susceptibility of molecular nanomagnets: tunneling of high-spin molecules, *Phys. Rev. B* **56** (1997) pp. 75-78.
35. Benelli C., Cano J., Journaux Y., Sessoli R., Solan G. A. and Winpenny R. E. P., A Decanuclear iron(III) single molecule magnet: use of Monte Carlo

methodology to model the magnetic properties, *Inorg. Chem.* **40** (2001) pp. 188-189.
36. Nakano M., Matsubayashi G.-E., Muramatsu T., Kobayashi T. C., Amaya K., Yoo J., Christou G. and Hendrickson D. N., Slow magnetization reversal in $[Ni_4(OMe)_4(sal)_4(MeOH)_4]$, *Mol. Cryst. Liq. Cryst.* **376** (2002) pp. 405-410.
37. Boskovic C., Wernsdorfer W., Folting K., Huffman J. C., Hendrickson D. N. and Christou G., Single-molecule magnets: novel Mn_8 and Mn_9 carboxylate clusters containing an unusual pentadentate ligand derived from pyridine-2,6-dimethanol, *Inorg. Chem.* **41** (2002) pp. 5107-5118.
38. Ochsenbein S. T., Murrie M., Rusanov E., Stoeckli-Evans H., Sekine C., Güdel H. U., Synthesis, Structure, and Magnetic Properties of the Single-Molecule Magnet $[Ni_{21}(cit)_{12}(OH)_{10}(H_2O)_{10}]^{16-}$, *Inorg. Chem.* **41** (2002) ASAP.
39. Barra A. L., Caneschi A., Cornia A., Fabrizi de Biani F., Gatteschi D. Sangregorio C., Sessoli R. and Sorace L., Single-molecule magnet behavior of a tetranuclear iron(III) complex. The origin of slow magnetic relaxation in iron(III) clusters, *J. Am. Chem. Soc.* **121** (1999) pp. 5302-5310.
40. Schenker R., Leuenberger M. N., Chaboussant G., Güdel H. U. and Loss D., Butterfly hysteresis and slow relaxation of the magnetization in $(Et_4N)_3Fe_2F_9$: manifestations of a single-molecule magnet, *Chem. Phys. Lett.* **358** (2002) 413-418.
41. Barra, A.-L., Brunel L.-C., Gatteschi D., Pardi L. and Sessoli R., High-frequency EPR spectroscopy of large metal ion clusters: from zero field splitting to quantum tunneling of the magnetization, *Acc. Chem. Res.* **31** (1998) pp. 460-466.
42. Cornia A., Gatteschi D. and Sessoli R., New experimental techniques for magnetic anisotropy in molecular materials, *Coord. Chem. Rev.* **219-221** (2001) pp. 573-604.
43. Wernsdorfer W., Classical and quantum magnetization reversal studied in nanometer-sized particles and clusters, *Adv. Chem. Phys.* **118** (2001) pp. 99-190.
44. Yang E.-C., Hendrickson D. N., Wernsdorfer W., Nakano M., Zakharov L. N., Sommer R. D., Rheingold A. L., Ledezma-Gairaud M. and Christou G., Cobalt single-molecule magnet, *J. Appl. Phys.* **91** (2002) pp. 7382-7384.
45. Gatteschi D. and Sorace L., Hints for the control of magnetic anisotropy in molecular materials, *J. Solid State Chem.* **159** (2001) pp. 253-261.
46. Entley W. R., Trentway C. R. and Girolami G. S., Molecular magnets constructed from cyanometalate building blocks, *Mol. Cryst. Liq. Cryst.* **273** (1995) pp. 153-166.
47. Weihe H. and Güdel H. U., Magnetic exchange across the cyanide bridge, *Comments Inorg. Chem.* **22** (2000) pp. 75-103.

48. Gadet V., Mallah T., Castro I. and Verdaguer M., High-T_C molecular-based magnets: a ferromagnetic bimetallic chromium(III)-nickel(II) cyanide with T_C = 90 K, *J. Am. Chem. Soc.* **114** (1992) pp. 9213-9214.
49. Mallah T., Thiébaut S., Verdaguer M. and Veillet P., High-T_C molecular-based magnets: ferrimagnetic mixed-valence chromium(III)-chromium(II) cyanides with T_C at 140 and 190 Kelvin, *Science* **262** (1993) pp. 1554-1557.
50. Entley W. R. and Girolami G. S., High-temperature molecular magnets based on cyanovanadate building blocks: spontaneous magnetization at 230 K, *Science* **268** (1995) pp. 397-400.
51. Ferlay S., Mallah T., Ouahès R., Veillet P. and Verdaguer M., A room-temperature organometallic magnet based on Prussian blue, *Nature* **378** (1995) pp. 701-703.
52. Dunbar K. R. and Heintz R. A., Chemistry of transition metal cyanide compounds: modern perspectives, *Prog. Inorg. Chem.* **45** (1997) pp. 283-391 and references therein.
53. Hatlevik Ø., Buschmann W. E., Zhang J., Manson J. L. and Miller J. S., Enhancement of the magnetic ordering temperature and air stability of a mixed valent vanadium hexacyanochromate (III) magnet to 99 °C (372 K), *Adv. Mater.* **11** (1999) pp. 914-918.
54. Holmes S. M. and Girolami G. S., Sol-gel synthesis of $KV^{II}[Cr^{III}(CN)_6]\cdot 2H_2O$: a crystalline molecule-based magnet with a magnetic ordering temperature above 100 °C, *J. Am. Chem. Soc.* **121** (1999) pp. 5593-5594.
55. Heinrich J. L., Berseth P. A. and Long J. R., Molecular Prussian blue analogues: synthesis and structure of cubic $Cr_4Co_4(CN)_{12}$ and $Co_8(CN)_{12}$ clusters, *Chem. Commun.* (1998) pp. 1231-1232.
56. Berseth P. A., Sokol J. J., Shores M. P., Heinrich J. L. and Long J. R., High-nuclearity metal-cyanide clusters: assembly of a $Cr_8Ni_6(CN)_{24}$ cage with a face-centered cubic geometry, *J. Am. Chem. Soc.* **122** (2000) pp. 9655-9662.
57. Klausmeyer K. K., Rauchfuss T. B. and Wilson S. R., Stepwise assembly of $[(C_5H_5)_4(C_5Me_5)_4Co_4Rh_4(CN)_{12}]^{4+}$, an "organometallic box", *Angew. Chem., Int. Ed. Engl.* **37** (1998) pp. 1694-1696.
58. Klausmeyer K. K., Wilson S. R. and Rauchfuss T. B., Alkali metal-templated assembly of cyanometalate "boxes" $(NEt)\{M[Cp^*Rh(CN)_3]_4[Mo(CO)_3]_4\}$ (M = K, Cs). Selective binding of Cs^+, *J. Am. Chem. Soc.* **121** (1999) pp. 2705-2711.
59. Yang J. Y., Shores M. P., Sokol J. J. and Long J. R., High-nuclearity metal-cyanide clusters: synthesis, magnetic properties, and inclusion behavior of open cage species incorporating $[(tach)M(CN)_3]$ (M = Cr, Fe, Co) complexes, *Inorg. Chem.* **42** (2003) in press.
60. Fehlhammer W. P. and Fritz M., Emergence of a CNH and cyano complex based organometallic chemistry, *Chem. Rev.* **93** (1993) pp. 1243-1280.
61. Sokol J. J., Shores M. P. and Long J. R., Giant metal-cyanide coordination

clusters: tetracapped edge-bridged cubic $Cr_{12}Ni_{12}(CN)_{48}$ and double face-centered cubic $Cr_{14}Ni_{13}(CN)_{48}$ species, *Inorg. Chem.* **41** (2002) pp. 3052-3054.

62. Larionova J., Gross M., Pilkington M., Andres H., Stoeckli-Evans H., Güdel H. U. and Decurtins S., High-spin molecules: a novel cyano-bridged $Mn^{II}_9Mo^{V}_6$ molecular cluster with a $S = {}^{51}/_2$ ground state and ferromagnetic intercluster ordering at low temperatures, *Angew. Chem., Int. Ed.* **39** (2000) pp. 1605-1609.
63. Zhong Z. J., Seino H., Mizobe Y., Hidai M., Fujishima A., Ohkoshi S. and Hashimoto K., A high-spin cyanide-bridged Mn_9W_6 cluster ($S = {}^{39}/_2$) with a full-capped cubane structure, *J. Am. Chem. Soc.* **122** (2000) pp. 2952-2953.
64. Scuiller A., Mallah T., Verdaguer M., Nivorozhin A., Tholence J. L. and Veillet P., A rational route to high-spin molecules via hexacyanometalates: a new □-cyano $Cr^{III}Mn^{II}_6$ heptanuclear complex with a low-lying $S = {}^{27}/_2$ ground state, *New J. Chem.* **20** (1996) pp. 1-3.
65. Parker R. J., Spiccia L., Berry K. J., Fallon G. D., Moubaraki B. and Murray K. S., Structure and magnetic properties of a high-spin $Mn^{II}_6Cr^{III}$ cluster containing cyano bridges and Mn centres capped by pentadentate ligands, *Chem. Commun.* (2001) pp. 333-334.
66. Bonadio F., Gross M., Stoeckli-Evans H. and Decurtins S., High-spin molecules: synthesis, X-ray characterization, and magnetic behavior of two new cyano-bridged $Ni^{II}_9Mo^{V}_6$ and $Ni^{II}_9W^{V}_6$ clusters with a $S = 12$ ground state, *Inorg. Chem.* **41** (2002) pp. 5891-5896.
67. Marvilliers A., Pei Y., Cano Boquera J., Vostrikova K. E., Paulsen C., Rivière E., Audière J.-P. and Mallah T., Metal-radical approach to high spin molecules: a pentanuclear □-cyano $Cr^{III}Ni^{II}(radical)_2$ complex with a low-lying $S = 9$ ground state, *Chem. Commun.* (1999) pp. 1951-1952.
68. Mallah T., Auberger C., Verdaguer M. and Vaillet P., A heptanuclear $Cr^{III}Ni^{II}_6$ complex with a low-lying $S = {}^{15}/_2$ ground state, *J. Chem. Soc., Chem. Commun.* (1995) pp. 61-62.
69. Vostrikova K. E., Luneau D., Wernsdorfer W., Rey P. and Verdaguer M., A $S = 7$ ground spin-state cluster built from three shells of different spin carriers ferromagnetically coupled, transition-metal ions and nitroxide free radicals, *J. Am. Chem. Soc.* **122** (2000) pp. 718-719.
70. Heinrich J. L., Sokol J. J., Hee A. G. and Long J. R., Manganese-chromium-cyanide clusters: molecular $MnCr_6(CN)_{18}$ and $Mn_3Cr_6(CN)_{18}$ species and a related $MnCr_3(CN)_9$ chain compound, *J. Solid State Chem.* **159** (2001) pp. 293-301.
71. Podgajny R., Desplanches C., Sieklucka B., Sessoli R., Villar V., Paulsen C., Wernsdorfer W., Dromzée Y., and Verdaguer M., Pentanuclear octacyanotungstate(V)-based molecule with a high-spin ground state $S = {}^{13}/_2$, *Inorg. Chem.* **41** (2002) pp. 1323-1327.
72. Marvilliers A., Hortholary C., Rogez G., Audière J.-P., Rivière E., Cano Boquera J., Paulsen C., Villar V. and Mallah T., Pentanuclear cyanide-bridged

complexes with high spin ground states S = 6 and 9: characterization and magnetic properties, *J. Solid State Chem.* **159** (2001) pp. 302-307.
73. Shores M. P., Sokol J. J. and Long J. R., Nickel(II)-molybdenum(III)-cyanide clusters: synthesis and magnetic behavior of species incorporating [(Me_3tacn)Mo($CN)_3$], *J. Am. Chem. Soc.* **124** (2002) pp. 2279-2292.
74. Miyasaka H., Matsumoto N., Okawa H., Re N., Gallo E. and Floriani C., Complexes derived from the reaction of manganese(II) Schiff base complexes and hexacyanoferrate(II): syntheses, multidimensional network structures, and magnetic properties, *J. Am. Chem. Soc.* **118** (1996) pp. 981-994.
75. Lescouëzec R., Vaissermann J., Lloret F., Julve M. and Verdaguer M., Ferromagnetic coupling between low- and high-spin iron(III) ions in the tetranuclear complex *fac*-{[Fe^{III}{$HB(pz)_3$}$(CN)_2$(□-CN)]$_3Fe^{III}(H_2O)_3$}·$6H_2O$ ($HB(pz)_2$)$^-$ = hydrotris(1-pyrazolyl)borate, *Inorg. Chem.* **41** (2002) pp. 5943-5945.
76. Van Langenberg K., Batten S. R., Berry K. J., Hockless D. C. R., Moubaraki B. and Murray K. S., Structure and magnetism of a bimetallic pentanuclear cluster [($Ni(bpm)_2)_3(Fe(CN)_6)_2$]·$7H_2O$ (bpm = bis(1-pyrazolyl)methane). The role of the hydrogen-bonded $7H_2O$ "cluster" in long-range magnetic ordering, *Inorg. Chem.* **36** (1997) pp. 5006-5015.
77. Van Langenberg K., Hockless D. C. R., Moubaraki B. and Murray K. S., Long-range magnetic order displayed by a bimetallic pentanuclear cluster complex [($Ni(2,2'\text{-bipy})_2)_3(Fe(CN)_6)_2$]·$13H_2O$ and a Cu(II) analog, *Synth. Met.* **122** (2001) pp. 573-580.
78. Kou H.-Z., Zhou B. C., Liao D.-Z., Wang R-J. and Li Y., From one-dimensional chain to pentanuclear molecule. Magnetism of cyano-bridged Fe(III)-Ni(II) complexes, *Inorg. Chem.* **41** (2002) pp. 6887-6891.
79. Oshio H., Yamamoto M., Ito T., Cyanide-bridged molecular squares with ferromagnetically coupled d□, d□, and p□ spin system, *Inorg. Chem.* **41** (2002) pp. 5817-5820.
80. Fu D. G., Chen J, Tan X. S., Jiang L. J., Zhang S. W., Zheng P. J. and Tang W. X., Crystal structure and magnetic properties of an infinite chainlike and a tetranuclear bimetallic copper(II)-chromium(III) complex with bridging cyanide ions, *Inorg. Chem.* **36** (1997) pp. 220-225.
81. Powell A. K., Heath S. L., Gatteschi D., Pardi L., Sessoli R., Spina G., Del Giallo F. and Pieralli F., Synthesis, structures, and magnetic properties of Fe_2, Fe_{17}, and Fe_{19} oxo-bridged iron clusters: the stabilization of high ground state spins by cluster aggregates, *J. Am. Chem. Soc.* **117** (1995) pp. 2491-2502.
82. Beauvais L. G. and Long J. R., Cyanide-limited complexation of molybdenum(III): synthesis of octahedral $[Mo(CN)_6]^{3-}$ and cyano-bridged $[Mo_2(CN)_{11}]^{5-}$, *J. Am. Chem. Soc.* **124** (2002) pp. 2110-2112.
83. Shores M. P. and Long J. R., Tetracyanide-bridged divanadium complexes: redox switching between strong antiferromagnetic and strong ferromagnetic

coupling, *J. Am. Chem. Soc.* **124** (2002) pp. 3512-3513.
84. Elbers G., Remme S. and Lehmann G., EPR of chromium(3+) in tris(acetylacetonato)gallium(III) single crystals, *Inorg. Chem.* **25** (1986) pp. 896-987.
85. Averill B. A. and Orme-Johnson W. H., Electron paramagnetic resonance spectra of molybdenum(III) complexes: direct observation of molybdenum-95 hyperfine interaction and implications for molybdoenzymes, *Inorg. Chem.* **19** (1980) pp. 1702-1705.
86. Friedman J. R., Sarachik M. P., Tejada J., Maciejewski J. and Ziolo R., Steps in the hysteresis loops of a high-spin molecule, *J. Appl. Phys.* **79** (1996) pp. 6031-6033.
87. Friedman J. R., Sarachik M. P., Tejada J. and Ziolo R., Macroscopic measurement of resonant magnetization tunneling in high-spin molecules, *Phys. Rev. Lett.* **76** (1996) pp. 3830-3833.
88. Sangregorio C., Ohm T., Paulsen C., Sessoli R. and Gatteschi D., Quantum tunelling of the magnetization in an iron cluster nanomagnet, *Phys. Rev. Lett.* **78** (1997) 4645-4648.
89. Barra A. L., Gatteschi D. and Sessoli R., High-frequency EPR spectra of $[Fe_8O_2(OH)_{12}(tacn)_6]Br$: a critical appraisal of the barrier for the reorientation of the magnetization in single-molecule magnets, *Chem. Eur. J.* **6** (2000) pp. 1608-1614.
90. Leuenberger M. N. and Loss D., Quantum computing in molecular magnets, *Nature* **410** (2001) pp. 789-793.
91. Tejada J., Chudnovsky E. M., del Barco E., Hernandez J. M. and Spiller T. P., Magnetic qubits as hardware for quantum computers, *Nanotechnology* **12** (2001) pp. 181-186.
92. Tejada J., Quantum behavior of molecule-based magnets: basic aspects (quantum tunneling and quantum coherence) and applications (hardware for quantum computers and magnetic refrigeration. A tutorial, *Polyhedron* **20** (2001) pp. 1751-1756.
93. Torres F., Hernández J. M., Bohigas X. and Tejada J., Giant and time-dependent magnetocaloric effect in high-spin molecular magnets, *Appl. Phys. Lett.* **77** (2000) pp. 3248-3250.